J|A|C|S
JOURNAL OF THE AMERICAN CHEMICAL SOCIETY

Article
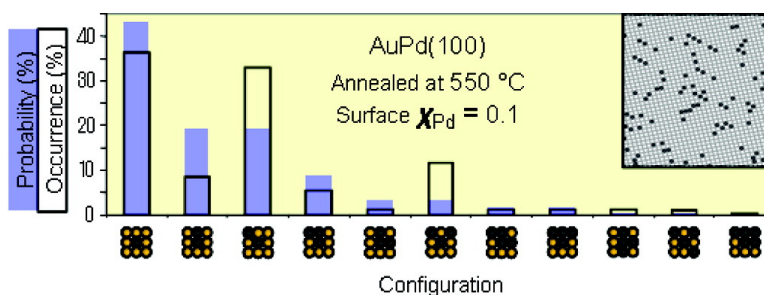
Atomic-Scale Assembly of a Heterogeneous Catalytic Site

Patrick Han, Stephanus Axnanda, Igor Lyubinetsky, and D. Wayne Goodman

More About This Article

Additional resources and features associated with this article are available within the HTML version:

- Supporting Information
- Links to the 2 articles that cite this article, as of the time of this article download
- Access to high resolution figures
- Links to articles and content related to this article
- Copyright permission to reproduce figures and/or text from this article

View the Full Text HTML

ACS Publications
High quality. High impact.

Atomic-Scale Assembly of a Heterogeneous Catalytic Site

Patrick Han,[†] Stephanus Axnanda,[†] Igor Lyubinetsky,[‡] and D. Wayne Goodman*,[†]

*Contribution from the Department of Chemistry, Texas A & M University,
College Station, Texas 77843-3255, and Pacific Northwest National Laboratory,
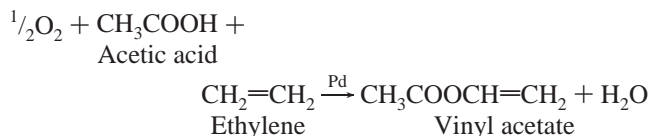EMSL, 902 Battelle Boulevard, P.O. Box 999, Richland, Washington 99352*

Received July 3, 2007; E-mail: goodman@mail.chem.tamu.edu

Abstract: The distance between surface Pd atoms has been shown to control the catalytic formation of vinyl acetate from ethylene and acetic acid by AuPd catalysts. Here, we use the bulk alloy's thermodynamic properties, as well as the surface lattice spacing of a AuPd(100) alloy single-crystal model catalyst to control and optimize the concentration of the active site (Pd atom pairs at a specific Pd–Pd distance with Au nearest-neighbors). Scanning tunneling microscopy reveals that sample annealing has a direct effect on the surface Pd arrangements: short-range order preferentially forms Pd pairs located in the $c(2 \times 2)$ sites, which are known to be optimal for vinyl acetate synthesis. This effect could be harnessed for future industrial catalyst design.

Introduction

Since one of the ultimate goals in heterogeneous catalysis is the design of novel catalysts from the nanoscale up, a fundamental understanding of the catalytic chemistry at the molecular- and atomic-scale is critical.[1] Recent advances in nanoscience have greatly contributed to this effect. Current tools useful to bottom-up catalyst design already include the control of the quantum-size effect by the dimensionality of the active nanoparticles.[2] In bimetallic catalysis, examples of these tools include the use of ligand effects to inhibit active-site poisoning[3] or the use of ensemble effects to facilitate the adsorption of specific reactant molecules.[4]

Recently, our group demonstrated that the active catalytic site for vinyl acetate (VA) formation

$$^1/_2O_2 + CH_3COOH +$$
<div align="center">Acetic acid</div>

$$CH_2{=}CH_2 \xrightarrow{Pd} CH_3COOCH{=}CH_2 + H_2O$$
<div align="center">Ethylene   Vinyl acetate</div>

on a Pd/Au(100) surface alloy is a Pd "monomer pair" with Au nearest-neighbors (Figure 1A). For this process, while a Au-isolated surface Pd atom is active for VA formation, the presence of a second Pd atom lowers the barrier for the step juxtaposing acetic acid and ethylene,[5] believed to be rate-limiting.[6,7] Therefore, the key aspect of ref 5 lies in the precise locations
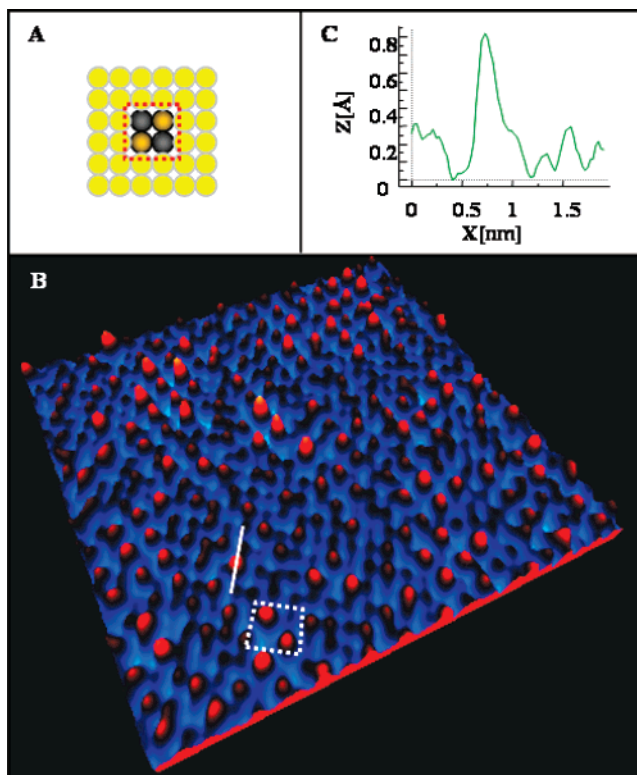

Figure 1. (A) Schematic representation of the catalytic site active to vinyl acetate formation referred to as "monomer pair" from ref 5 (red dotted square). This configuration is closely related to the $c(2 \times 2)$ structure on a metal fcc(100) surface. (B) 3D-view of an STM image (7.7 nm × 7.7 nm, $V_s = -10$ mV, $I_t = 5.0$ nA) of the AuPd(100) bulk alloy. The white dotted square highlights an example of the targeted Pd monomer pair. (C) Height trace of a Pd atom surrounded by Au atoms. The location of (C) is shown as a white line in (B).

of the surface atomic species. To maximize the activity enhancement for VA formation, the optimum distance between Pd atoms within a single catalytic site is predicted to be 0.33

† Texas A & M University.
‡ Pacific Northwest National Laboratory.
(1) Bell, A. T. *Science* **2003**, *299*, 1688.
(2) Valden, M.; Lai, X.; Goodman, D. W. *Science* **1998**, *281*, 1647.
(3) Besenbacher, F.; Chorkendorff, I.; Clausen, B. S.; Hammer, B.; Molenbroek, A. M.; Norskov, J. K.; Stensgaard, I. *Science* **1998**, *279*, 1913.
(4) Maroun, F.; Ozanam, F.; Magnussen, O. M.; Behm, R. J. *Science* **2001**, *293*, 1811.
(5) Chen, M. S.; Kumar, D.; Yi, C. W.; Goodman, D. W. *Science* **2005**, *310*, 291.
(6) Nakamura, S.; Yasui, T. *J. Catal.* **1970**, *17*, 366.
(7) Samanos, B.; Boutry, P.; Montarna. R *J. Catal.* **1971**, *23*, 19.
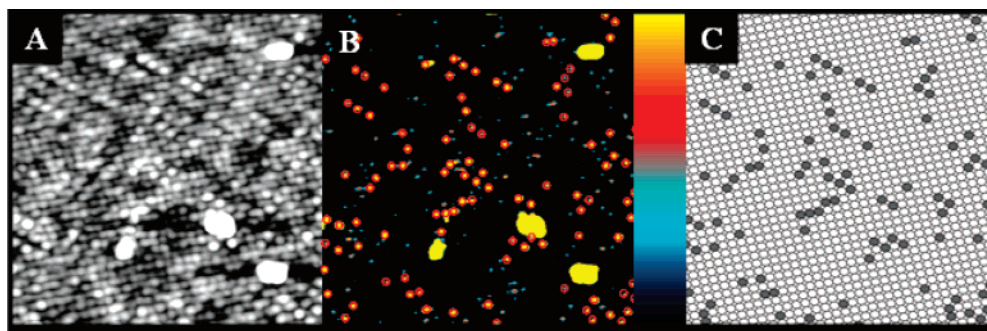
Figure 2. (A) STM image of a AuPd(100) bulk alloy (10 nm × 10 nm, V_s = −15 mV, I_t = 6.3 nA). The large white features are impurities thought to be carbon (Auger electron spectroscopic measurement of the surface showed no visible signal of C, S, O, K, or Ca). (B) The same STM image as that in (A) excluding all data points below the cutoff height, which is set to 5 pm below the highest point of the image. The color bar scale spans from 0 to 5 pm. The red circles denote the features designated to be Pd atoms. These red circles are set to have an area of ∼0.15 nm². (C) Schematic representation of (A) for clarity.

nm, while the two atoms shared as nearest-neighbors by the Pd atoms must be Au atoms. This catalytic site structure is best modeled by the c(2 × 2)-like configuration on a (100) surface shown in Figure 1A, which has a Pd−Pd distance of 0.41 nm.

Here, we use ultrahigh vacuum (UHV) scanning tunneling microscopy (STM) to image the Pd monomer pair on a AuPd-(100) bulk alloy surface, to target the Pd monomer-pair active site. Moreover, we present a method for increasing the concentration of active sites that relies on the thermodynamic properties of binary solid mixtures.[8] We demonstrate that, by choosing a bulk alloy of specific composition, and by using a specific crystal preparation method, it is possible to influence the atomic arrangement within the AuPd(100) surface lattice, maximizing the concentration of this desired active site. The validity of this concept is tested by comparing the Pd distribution on our surface with that of a previously imaged Au₃Pd(100) surface prepared differently by Achoff et al.[9] This method of globally controlling the lateral distribution of metal atoms at the atomic scale has important implications in bimetallic catalysis and other alloy technologies. Its usefulness extends to any field that requires a bottom-up approach to nanoscale surface structures.[10−12]

Experimental Section

The experiments were performed in two UHV chambers. The first chamber is equipped with an STM (Omicron VT-STM), a semispherical electron energy analyzer (VG), a mass spectrometer (Ametek), and electron and ion guns (VG and SPECS, respectively). A base pressure of 5 × 10⁻¹¹ Torr was maintained. All STM images were acquired at room temperature, in constant current mode, using an electrochemically etched W tip. The AuPd(100) bulk alloy single crystal was purchased from Matek, and the ordered surface was obtained through repeated sputter and anneal cycles (E = 500 eV, I = 0.38 μA, Ar⁺ sputtering at room temperature for 20 min, annealing at ∼550 °C for 15 min). The sample was annealed without sputtering at 550 °C for 30 min before imaging and was allowed to cool to room temperature without deliberate temperature quenching. The surface temperature was measured optically by infrared pyrometry.

The second chamber is equipped with low-energy ion scattering spectroscopy (LEISS), X-ray photoelectron spectroscopy, temperature programmed desorption, and low-energy electron diffraction (LEED) with a base pressure of 5 × 10⁻¹⁰ Torr. For the LEISS experiments, the sample was heated resistively. The temperature was measured using a C-type thermocouple (W-5%Re/W-26%Re) spot welded to the backside of the sample. LEISS experiments were carried out using a He⁺ beam with an energy of 1000 eV and an incident angle of ∼45° from the surface normal. The LEISS spectra were collected using a concentric hemispherical analyzer and were acquired at room temperature. The sample was treated with the same cleaning procedure used in the first chamber before LEISS experiments were done. The surface concentrations of Au (c_{Au}) from the AuPd alloy were calculated using the following equation:[13]

$$c_{Au} = I_{Au}/(I_{Au} + f_{Au/Pd} \cdot I_{Pd}) \tag{1}$$

where $f_{Au/Pd}$ is the ratio of the scattering intensity for pure Au and Pd, and I_{Au} and I_{Pd} are the scattering intensity from Au and Pd from the alloy surface, respectively.

Results and Discussion

Imaging the AuPd(100) surface with atomic resolution reveals a chemical contrast between Pd and Au surface atoms.[14] Figure 1B shows a Fourier-filtered STM image of the surface. The white dotted square highlights a Pd monomer pair, the targeted active site (highlighted in Figure 1A by a red dotted square). The chemical contrast is explained by the difference in the local electronic density of states near the Fermi edge between Pd and Au atoms.[15] This effect is further enhanced by STM tips with a specific type of apex prone to an increased interaction with Pd, the more reactive surface species.[15] Based on this and previous STM work on a Au₃Pd(100) bulk alloy,[9] we assign the higher protrusions in Figure 1B to Pd atoms. Typically, the apparent-height difference associated with the chemical contrast for alloy surfaces ranges from 10 to 60 pm,[15] with very narrow apparent-height distributions for each metallic species. Our observed height difference between Pd and Au surface atoms falls within this range (Figure 1C).

(8) Gordon, P. The Order-Disorder Transformation. *Principles of Phase Diagrams in Material Systems*; McGraw-Hill: New York, 1968; p 107.
(9) Aschoff, M.; Speller, S.; Kuntze, J.; Heiland, W.; Platzgummer, E.; Schmid, M.; Varga, P.; Baretzky, B. *Surf. Sci.* **1998**, *415*, L1051.
(10) Hatzor, A.; Weiss, P. S. *Science* **2001**, *291*, 1019.
(11) Roder, H.; Hahn, E.; Brune, H.; Bucher, J. P.; Kern, K. *Nature* **1993**, *366*, 141.
(12) Tseng, G. Y.; Ellenbogen, J. C. *Science* **2001**, *294*, 1293.

(13) Niehus, H.; Heiland, W.; Taglauer, E. *Surf. Sci. Rep.* **1993**, *17*, 213.
(14) Hebenstreit, E. L. D.; Hebenstreit, W.; Schmid, M.; Varga, P. *Surf. Sci.* **1999**, *441*, 441.
(15) Schmid, M.; Varga, P. Segregation and surface chemical ordering - an experimental view on the atomin scale. In *The Chemical Physics of Solid Surfaces: Alloy Surface and Surface Alloys*; Woodruff, D. P., Ed.; Elsevier Science: New York, 2002; Vol. 10, p 118.
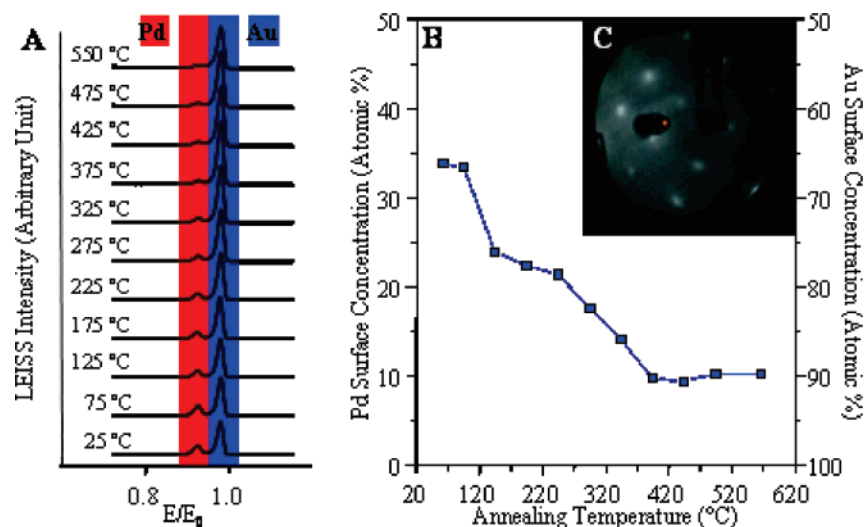
Figure 3. (A) Low-energy ion scattering spectra of AuPd(100) as a function of temperature. Each spectrum was collected at 25 °C after the sample was annealed to the indicated temperature. The spectrum at 25 °C was collected immediately after sputtering at 25 °C. (B) Surface concentration of Pd on AuPd(100) as a function of annealing temperature. Except at 25 °C, the sample was annealed at each temperature for 10 min. The low Pd surface composition at 25 °C may be a result of surface segregation at this temperature. It should be noted that, in a separate LEISS experiment, annealing the sample at 550 °C for 3 × 10 min showed no change in Pd surface concentration: we conclude that the Pd surface concentration reaches equilibrium after 10 min. (C) Low-energy electron diffraction of AuPd(100) after the last annealing of the sample at 550 °C, showing the fcc(100)-(1 × 1) square pattern.

Aside from the contrast between Au and Pd, the entire surface is also modulated by the electronic contribution of subsurface atoms.[16] This is apparent in Figure 2A, which shows an unfiltered STM image of the AuPd(100) surface. Here, a disparity in apparent height is observable between atoms of the same species.

Since the exact location of each surface Pd atom is critical to surface Pd distribution measurement, we use unprocessed STM data for Pd assignment. Due to the convolution of both chemical contrast and the electronic contribution of the subsurface atoms, the following method was used to distinguish Pd from Au atoms. To designate the surface Pd atoms, all data points of the image in Figure 2A below a cutoff height are shown uniformly in black in Figure 2B. The cutoff height chosen is 5 pm below the highest surface atom (impurities are not included in the process). Any remaining bright spots in Figure 2B that have a surface area of ~0.15 nm^2 are designated as Pd atoms. Local profile measurements are performed to ensure correct assignments (Figure 1C). All surface atoms are then counted, giving 103 Pd atoms out of a total of 1287 surface atoms (8% Pd). This is in good agreement with our LEISS measurements (10% Pd at 550 °C annealing temperature, Figure 3). Figure 2C shows a schematic representation of the STM image shown in Figure 2A for clarity.[17] This analysis is performed for three STM images acquired over different regions of the surface.

To analyze the distribution of the surface Pd atoms, we compare the observed distribution with a calculated random distribution.[18] $P(C)$, the probability of a surface Pd atom having its eight nearest-neighbors arranged in a specific configuration C (shown on the abscissa of Figure 4), is calculated

assuming a complete random distribution. The following equation is used

$$P(C) = m(\rho_{Pd}{}^n \times \rho_{Au}{}^{(8-n)}), \qquad 0 \le n \le 8 \qquad (2)$$

where ρ_{Pd} and ρ_{Au} are the probabilities of finding a Pd and Au surface atom, respectively, m is the number of degenerate configurations, and n is the number of nearest-neighbor Pd atoms. For a complete random distribution, $P(C)$ depends only on the surface concentration of each metal. Therefore, the respective surface mole fractions observed by LEISS ($\chi_{Au} = 0.9$, $\chi_{Pd} = 0.1$) can be used as ρ_{Au} and ρ_{Pd} for AuPd(100). The results of the first 11 most probable configurations are displayed in Figure 4 as solid blue bars. A complete list of calculated $P(C)$ for $\chi_{Pd} = 0.1$ as well as the systematic method used to categorize them can be found in Figure 5. The same $P(C)$ calculation is performed for the image acquired previously by Achoff et al.[9] Here, the mole fractions ($\chi_{Au} = 0.86$, $\chi_{Pd} = 0.14$) measured directly from the image are used. It should be noted that each configuration shown in Figure 4 represents one of many equivalent configurations. A list of all possible configurations can be found in Figure S1 of the Supporting Information.

For the observed distribution, Pd atoms of the same and equivalent eight nearest-neighbor configurations are totaled as occurrences, which are displayed on top of the respective calculated probabilities as transparent bars in Figure 4. For Figure 4A, this was done for a single image acquired previously by Aschoff et al.[9] For Figure 4B, each occurrence is the average of the respective measurements of three STM images (all 10 nm × 10 nm) acquired over different surface regions. The individual measurements of these images are also displayed in Figure 4B as colored triangles. All probabilities and occurrences are normalized and shown as percentages. No Pd with $C > 11$ is observed.

The charts in Figure 4 illustrate that the two surfaces of interest have markedly different Pd distributions. The distribu-

(16) Wouda, P. T.; Schmid, M.; Nieuwenhuys, B. E.; Varga, P. *Surf. Sci.* **1998**, *417*, 292.

(17) It should be noted that this method may underestimate the number of surface Pd atoms, as the cutoff height is set relatively high above the surface to avoid any accidental inclusion of Au atoms.
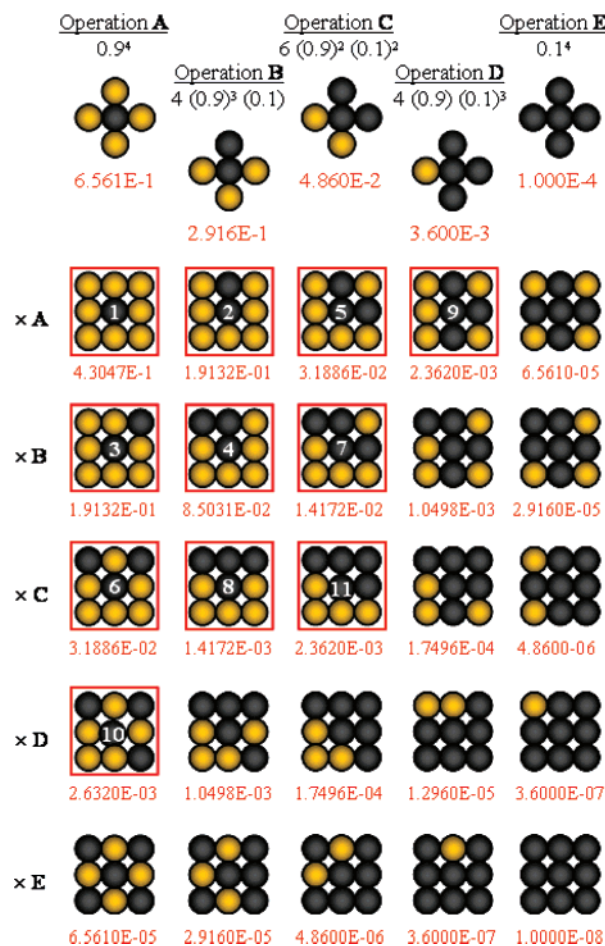
(18) Han, P.; Mantooth, B. A.; Sykes, E. C. H.; Donhauser, Z. J.; Weiss, P. S. *J. Am. Chem. Soc.* **2004**, *126*, 10787.
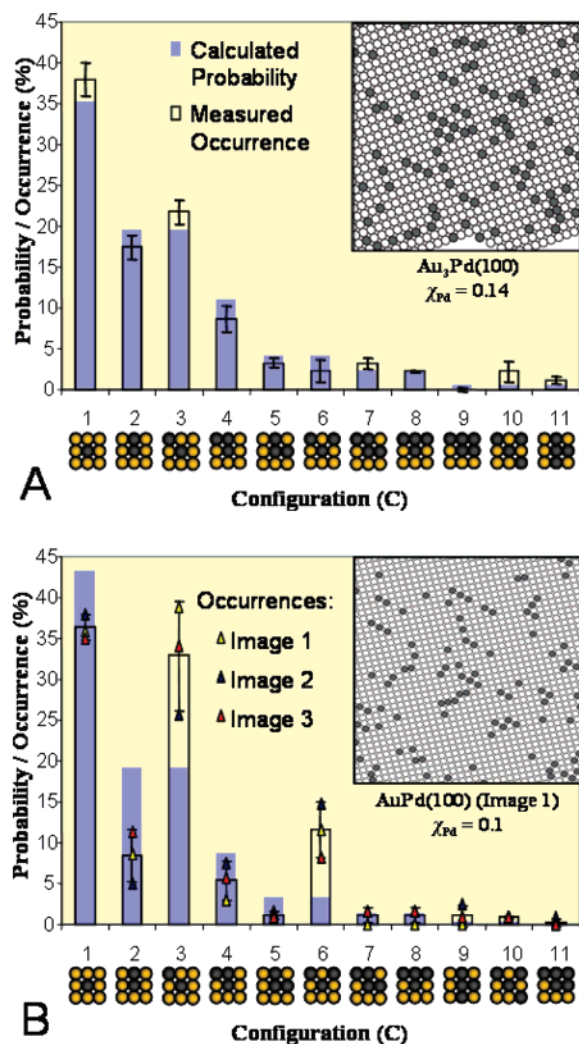
Figure 4. Comparison between calculated probability and observed occurrence of specific nearest-neighbor configurations around a Pd atom. The chart in (A) shows the Pd distribution from the STM image (7.9 nm × 7.9 nm) acquired previously by Achoff et al. over a Au$_3$Pd(100) surface[9] (schematic representation in the inset). Error bars in (A) show the standard deviations between the calculated probabilities and measured occurrences. The chart in (B) shows the Pd distributions of the AuPd(100) surface. Each measured occurrence in (B) is the averaged value of respective measurements made on three STM images (10 nm × 10 nm) acquired over different surface regions. The occurrence measurement of each image is also shown as triangles. Error bars in (B) show the standard deviations of the averaging process. The inset in (B) shows a representative schematic of the three STM images. All calculated probabilities and occurrences are normalized. The Pd mole fractions used for the probability calculation is measured by STM in (A) and by LEISS in (B).

Figure 5. Calculation of the probability of finding a Pd surface atom surrounded by its eight nearest-neighbors in a specific configuration, using eq 2 (see text). The calculations are made for a surface with 0.9 ML Au and 0.1 ML Pd, assuming a complete random distribution. The top row of the figure shows the schematic of the configurations with the first four nearest-neighbors only. Operations A−D used to calculate the probabilities are shown in black above the schematics, and the resulting probabilities are shown in red below the schematics. The bottom of the figure lists the probability calculation including the next four nearest-neighbors. The red squares indicate the 11 configurations with the highest probabilities. These are the configurations listed along the x-axis in both Figures 4 and 6. The numbers on the central Pd atoms assign the descending order of calculated probability magnitude.

tion of Au$_3$Pd(100) (Figure 4A) follows the calculated random distribution quite well, while the distribution of AuPd(100) (Figure 4B) shows a clear preference for configurations 3 and 6, both of which involve Pd atoms arranged in local c(2 × 2)-like structures exclusively. The occurrences of all other configurations in Figure 4B are well below the calculated random probabilities.

Figure 4 also provides a sense of uniformity of the AuPd-(100) Pd surface distribution. While only a single STM image is used to compile Figure 4A, three images acquired over different surface regions are used to compile Figure 4B to compensate for the local nature of STM. From the individual occurrence measurements (colored triangles in Figure 4B), it is clear that the preference for configurations 3 and 6 is present

over all three regions. Moreover, focusing on configurations 3 and 6, a higher count of one configuration is accompanied by a lower count of the other. This is an indication that the number of monomer-pair active sites (Figure 1A) is also uniform across the surface. A monomer-pair count for each image yields 35, 36, and 29 sites for Images 1−3, respectively, averaging to 33 ± 4 sites/100 nm^2. It should be noted that the standard deviation of this average monomer-pair count is well within experimental error, as the actual configuration for Pd atoms located at the edge of the STM images is unknown.

A similar monomer-pair count for the image of Au$_3$Pd(100)[9] yields 25 sites/100 nm^2. Taking into account the surface Pd composition, the number of monomer-pair sites per surface Pd atom amounts to 0.27 and 0.15 sites/Pd for AuPd(100) and Au$_3$-Pd(100), respectively. From these observations, we conclude that the AuPd(100) surface presented here has a uniform, nonrandom Pd surface distribution with a preference for local c(2 × 2)-like Pd arrangements. Per surface Pd atom, this type of Pd surface distribution yields almost twice the number of
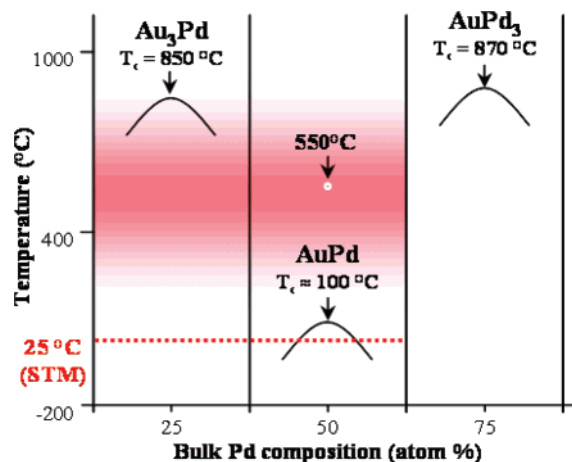
Figure 6. Partial temperature−composition phase diagram of AuPd solid solutions based on ref 20, below the melting point. The curved lines show the order−disorder phase boundaries of the alloy at various compositions. The red shaded area represents the usual sample annealing temperature range during sample preparation. This temperature range encompasses the actual annealing temperatures for both AuPd(100) from this work and Au₃Pd-(100) from ref 9. The white circle in the AuPd phase indicates the actual annealing temperature for the AuPd(100) sample preparation in this work. The red dotted line shows room temperature, at which all STM images were acquired.

the targeted Pd monomer-pair sites when compared with a surface with random Pd distribution.

To demonstrate the relevance of our findings, it is important to understand the order−disorder transformations in binary bulk alloy single crystals.[8] For these solid solutions, the terms "order" and "disorder" do not refer to the crystal lattice but are used to describe the relative arrangement of the two atomic species within the lattice. More specifically, complete disorder means that the probability for an atom of species x finding a neighboring atom of species y at a specific distance d ($P(x,y,d)$) is random ($P(random)$), while a higher degree of order means a significant deviation of $P(x,y,d)$ from $P(random)$. This type of chemical ordering is a function of thermodynamics and is dependent on the atomic size of the metal components, as well as the interatomic interactions between the components.[19]

In solid solutions there are two types of chemical order, namely short-range order (SRO) and long-range order (LRO).[8] The distinction between the two is first a spatial one. From the atomic perspective, if the deviation of $P(x,y,d)$ from $P(random)$ drops rapidly with distance, the order is short-range. For LRO, the deviation of $P(x,y,d)$ from $P(random)$ must remain constant for a long enough distance such that the symmetry of the crystal is lowered. Therefore, it follows that LRO can be detected in X-ray diffraction (XRD) data as superlattice reflections. SRO, which only affects the background scattering of XRD, is usually measured by X-ray diffuse scattering (XDS).

A second distinction between SRO and LRO is thermodynamic in origin. LRO is only present below a critical temperature (T_c), while SRO may or may not exist above T_c. This is illustrated by the phase diagram in Figure 6.[20] While the two types of order relate to bulk binary alloys, the same ideas can be applied to their surfaces, as both LRO and SRO had been previously observed by proximal probes.[21−23]

The different surface Pd distributions of AuPd(100) and Au₃-Pd(100) result from two factors, namely bulk composition and surface preparation. This point is illustrated by the red shaded area in Figure 6. The red shaded area indicates the usual annealing temperature range for metal crystal preparation, which falls between the T_c of both AuPd and Au₃Pd. For the AuPd-(100) in this work, the sample was sputtered at room temperature and annealed at 550 °C without sputtering for 30 min to allow equilibration before imaging at room temperature. The low concentration of surface Pd (10%) is due to Au surface segregation caused by the difference in the surface energies of the metallic species.[15] The equilibration time allows both surface segregation and SRO to reach completion, explaining the deviation of the observed Pd surface distribution from the calculated random distribution (Figure 3B). The fact that the sample was annealed above T_c has a crucial thermodynamic implication; i.e., the sample preparation method excludes the presence of LRO but permits SRO, as shown in our STM images.[24]

Due to its lower bulk Pd concentration, a similar treatment of a Au₃Pd(100) sample yields a surface free of Pd atoms,[9] instead of the desired long-range c(2 × 2) structure as suggested by Figure 6, which indicates LRO at the preparation temperatures below T_c. To counteract the effects of Au surface segregation, Aschoff et al. used differential sputtering, consisting of sputtering the surface while annealing, preferentially removing the surface segregated species.[25] In the case of Au₃Pd(100), Au is preferentially removed, leaving the layers near the surface Pd-rich. During sample cooling, Au atoms resurface by diffusion, but the process is quenched before both surface segregation and SRO can reach equilibrium. The random distribution of surface Pd atoms seen in Figure 4A reflects this process.

From these observations, we propose that the thermodynamic properties of AuPd alloys can be used to tailor surface ordering. Choosing the (100) face of the bulk alloy allows for the formation of Pd pairs of the right distance for promoting VA formation; opting for a higher bulk Pd composition reduces the effects of surface segregation. In addition, the unusually low T_c of AuPd (Figure 6) provides a wide temperature range where regular crystal preparation methods can be used to fine-tune the degree of surface SRO. To this end, our LEISS data indicate that the Pd surface concentration does not decrease monotonically with increasing annealing temperature but does so in a stepwise fashion. Figure 3B shows there is no significant change in surface Pd concentration for annealing temperatures ranging from 375 to 550 °C. However, the degree of SRO within this temperature range had been previously demonstrated by XDS to be temperature-dependent.[26] According to Ivernova et al., the degree of SRO in a AuPd 1:1 mixture increases with temperature from T_c to peak near 500 °C. This means that on a (100) surface of a AuPd 1:1 bulk alloy, both the activity and selectivity for catalytic reactions such as VA synthesis can be systematically controlled. We have shown that annealing the

(19) Guczi, L. *Catal. Today* **2005**, *101*, 53.
(20) Okamoto, H.; Massalski, T. B. *Bull. Alloy Phase Diagrams* **1985**, *6*, 229.
(21) Gauthier, Y.; Dolle, P.; Baudoing-Savois, R.; Hebenstreit, W.; Platzgummer, E.; Schmid, M.; Varga, P. *Surf. Sci.* **1998**, *396*, 137.
(22) Niehus, H.; Baumann, T.; Voetz, M.; Morgenstern, K. *Surf. Rev. Lett.* **1996**, *3*, 1899.
(23) Rodewald, M.; Rodewald, K.; DeMeulenaere, P.; VanTendeloo, G. *Phys. Rev. B* **1997**, *55*, 14173.
(24) Although no deliberate quenching was performed, we assume that all processes involving atomic rearrangement have undetectable relaxation time during STM imaging at room temperature.
(25) Swartzfager, D. G.; Ziemecki, S. B.; Kelley, M. J. *J. Vac. Sci. Technol.* **1981**, *19*, 185.
(26) Ivernova, V. I.; Katsnel'son, A. A. *Sov. Phys. Crystallogr.* **1967**, *11*, 504.
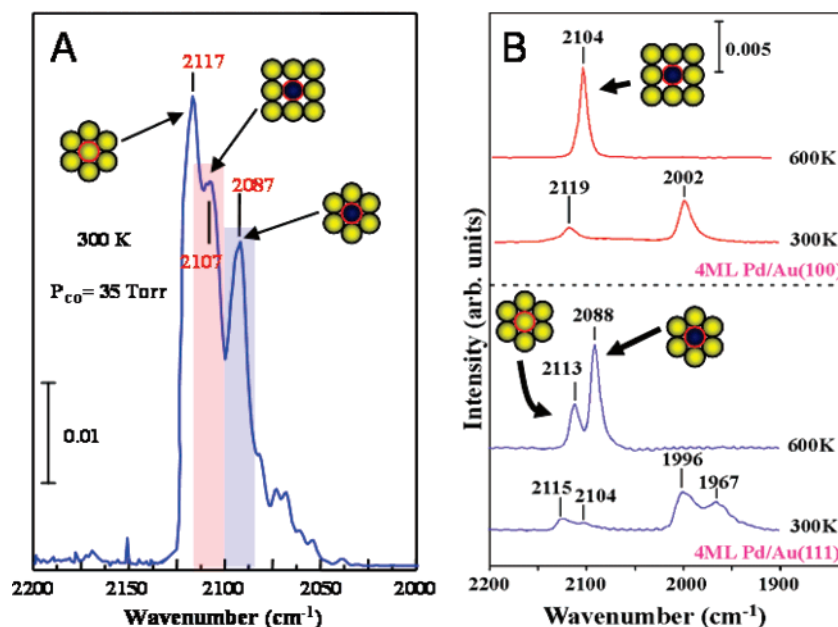
Figure 7. Infrared reflection absorption spectra for CO adsorption on: (A) SiO$_2$ supported AuPd catalyst; and (B) 4 ML Au on Pd(100) (top) and 4 ML Au on Pd(111) (bottom). Based on the assignments in (B) the signals at 2117 and 2087 cm^{-1} in (A) are assigned to CO adsorbed on Au and Pd within a (111) facet of AuPd alloy crystallites, respectively. Accordingly the signal at 2107 cm^{-1} is assigned to CO adsorbed on Pd within a (100) facet of AuPd alloy crystallites. The spectrum in (A) was acquired at 300 K with a background CO pressure of 35 Torr. Details of the spectra in (B) for CO adsorption on Pd/Au(111) and Pd/Au(100) can be found in ref 5.

crystal between 375 and 550 °C yields a surface with 10% surface Pd atoms. In principle, within this temperature range, the degree of SRO, i.e., the number of desired catalytic sites, can be maximized by a specific annealing temperature. Further work is needed to determine the ideal temperature.

It should be noted that the temperature–composition phase diagram shown in Figure 6 only addresses the bulk of the AuPd alloys. In addition, it is well-known that the concentration profile near the surface of a bulk binary alloy is not uniform due to surface segregation.[27] This brings up the possibility that the phase diagram of the alloy surface might be different from that of the bulk. However, although the exact relationship between the thermodynamic properties of the surface and that of the bulk cannot be inferred directly, this work demonstrates that such a relationship not only does exist, at least for the AuPd system, but it can also be utilized for enhancing the concentration of targeted active sites.

With regard to industrial AuPd catalysts, the formation of AuPd alloy crystallites had been previously demonstrated by XRD and transmission electron microscopy.[28,29] Furthermore, our group had verified the presence of both (111) and (100) facets of these AuPd alloy crystallites by infrared reflection adsorption spectroscopy on an industrial-like SiO$_2$-supported AuPd catalyst[30] (Figure 7). Based on this and our present observations, we propose that the role of the Au promoter in Au–Pd catalysts is twofold. First, the inert Au atoms separate the Pd surface atoms spatially, making the formation of Pd monomer-pair active sites with a 0.41 nm Pd–Pd distance possible over the (100) alloy crystal facets.[5] Second, the number

of monomer pairs at the surface is thermodynamically controlled by the bulk crystallinity, bulk composition, and catalyst temperature (throughout the life span of the catalyst). Therefore, in light of our proposed mechanism, further improvement is possible to optimize not only the reaction rate but also the selectivity of industrial AuPd catalysts. Fine-tuning the thermodynamic parameters can potentially change the degree of SRO, while leaving the total surface Pd atoms unchanged.[31] Finally, since this proposed mechanism relies exclusively on the fundamental thermodynamics of binary mixtures, the role of SRO, LRO, and surface segregation may be extensive in alloy catalysts. The control of SRO is a means of controlling the degree of randomness of the surface atomic distribution and, therefore, can be used to enhance other desired effects such as the ligand effect in a Ni/Au bulk alloy system[3] or the ensemble effect in Pd/Au bulk alloy systems.[4,5] These results have implications not only to mixed-metal catalysis but also to other technologies that rely on an atomic-level approach to alloy surface structures such as molecular self-assembly and molecular devices.[10–12]

Conclusion

We have used a combination of STM and LEISS to demonstrate that the surface Pd distribution of a AuPd(100) bulk alloy surface can be controlled by its thermodynamic properties. By choosing the bulk composition and preparation method of an fcc (100) bulk alloy single crystal, we have targeted a catalytic site of known atomic structure and have increased the coverage of the desired site known to enhance VA formation.[5] This effect is further confirmed by comparing the Pd surface distribution of our surface with that of a previously imaged

(27) Stamenkovic, V. R.; Fowler, B.; Mun, B. S.; Wang, G. F.; Ross, P. N.; Lucas, C. A.; Markovic, N. M. *Science* **2007**, *315*, 493.

(28) Han, Y. F.; Wang, J. H.; Kumar, D.; Yan, Z.; Goodman, D. W. *J. Catal.* **2005**, *232*, 467.

(29) Persson, K.; Ersson, A.; Jansson, K.; Iverlund, N.; Jaras, S. *J. Catal.* **2005**, *231*, 139.

(30) Bissot, T. C. U.S. Patent 4,048,096, 1977.

(31) It should be noted that at the thermodynamic properties of alloy nanoparticles might be considerably different from those of the alloy single crystal. Further investigation on the order–disorder transformation of alloy nanoparticles is necessary.

AuPd(100) prepared with a different scheme that favors a random Pd distribution.[9] Our method of assembling a targeted catalytic site is an additional tool toward bottom-up catalyst design.

Note Added after ASAP Publication. There was a production error in the version published on the Internet on October 30, 2007. In the print version and in the version published on the Internet on November 9, 2007, the formula for vinyl acetate is correct in the equation on the first page.

Supporting Information Available: Schematic showing the complete listing of equivalent configurations in each group highlighted by red squares in Figure 5 (Figure S1). This material is available free of charge via the Internet at http://pubs.acs.org.

JA074891N